Ocean Dynamics (2013) 63:865–880
DOI 10.1007/s10236-013-0632-2

Simulations of a Line W-based observing system for the Atlantic meridional overturning circulation

Matthias Fischer · Arne Biastoch · Erik Behrens · Johanna Baehr

Received: 7 August 2012 / Accepted: 3 June 2013 / Published online: 28 June 2013
© Springer-Verlag Berlin Heidelberg 2013

Abstract In a series of observing system simulations, we test whether the Atlantic meridional overturning circulation (AMOC) can be observed based on the existing Line W deep western boundary array. We simulate a Line W array, which is extended to the surface and to the east to cover the basin to the Bermuda Rise. In the analyzed ocean circulation model ORCA025, such an extended Line W array captures the main characteristics of the western boundary current. Potential trans-basin observing systems for the AMOC are tested by combining the extended Line W array with a mid-ocean transport estimate obtained from thermal wind "measurements" and Ekman transport to the total AMOC (similarly to Hirschi et al., Geophys Res Lett 30(7):1413, 2003). First, we close Line W zonally supplementing the western boundary array with several "moorings" in the basin (Line W-32°N). Second, we supplement the western boundary array with a combination of observations at Bermuda and the eastern part of the RAPID array at 26°N (Line W-B-RAPID). Both, a small number of density profiles across the basin and also only sampling the eastern and western boundary, capture the variability of the AMOC at Line W-32°N and Line W-B-RAPID. In the analyzed model, the AMOC variability at both Line W-32°N and Line W-B-RAPID is dominated by the western boundary current variability. Away from the western boundary, the mid-ocean transport (east of Bermuda) shows no significant relation between the two Line W-based sections and 26°N. Hence, a Line W-based AMOC estimate could yield an estimate of the meridional transport that is independent of the 26°N RAPID estimate. The model-based observing system simulations presented here provide support for the use of Line W as a cornerstone for a trans-basin AMOC observing system.

Keywords Atlantic meridional overturning circulation · Observing system simulations · Line W · RAPID

Responsible Editor: Dirk Olbers

M. Fischer (✉) · J. Baehr
Institute of Oceanography, KlimaCampus, University of Hamburg, Bundesstr. 53, 20146 Hamburg, Germany
e-mail: matthias.fischer@zmaw.de

A. Biastoch · E. Behrens
GEOMAR Helmholtz-Zentrum für Ozeanforschung Kiel, Kiel, Germany

1 Introduction

The Atlantic meridional overturning circulation (AMOC) plays a key role in the meridional transport of heat and freshwater. The AMOC is defined by the zonally and vertically integrated meridional flow as a function of latitude. Observing the AMOC therefore requires a continuous estimate of meridional velocity field across a zonal transect. Until the start of the 26°N Rapid Climate Change-Meridional Overturning Circulation and Heat Flux array (RAPID/MOCHA) in March 2004 (Kanzow et al. 2007; Cunningham et al. 2007), no measurement of the AMOC with the ability to monitor long-term variations has been obtained due to lack of adequate data. The AMOC estimate from the RAPID/MOCHA array is a sum of several individually measured components of the AMOC, namely the western boundary current (WBC), the Ekman transport, and a mid-ocean component between Bahamas and West Africa. The time mean AMOC and its standard deviation (STD) obtained from 10-day low-pass-filtered RAPID/MOCHA observations between April 2004 and April 2008 is 18.7 ± 2.1 Sv (1 Sv = 10^6 m^3/s; Kanzow et al. 2010).

Recently, a further estimate of the AMOC at around 41°N was obtained, based on profiling floats above 2,000 m showing an AMOC of 15.5 Sv ± 2.4 Sv (time mean value ± root-mean-square error (RMSE); Willis 2010).

Apart from RAPID/MOCHA, various observing systems exist measuring components of the AMOC (Cunningham and et al. 2010). However, none of these arrays apart from RAPID/MOCHA covers the full basin to provide continuous observations of the total AMOC raising the question how representable the AMOC estimate of RAPID/MOCHA is for other latitudes, as first raised by Bingham et al. (2008). One observing array that focusses on the observation of the Deep Western Boundary Current (DWBC) is Line W. The program covers the continental slope between New England and Bermuda with moored arrays and repeated shipboard measurements underlying a satellite ground track (Toole et al. 2011). While Line W is currently measuring one component of the AMOC, reconstructing the full AMOC would require an estimate of the flow in the interior.

In the present study, we test potential observing systems for the AMOC extending Line W via Bermuda to capture a basin-wide meridional flow. To test these potential observing systems, we deploy them into a numerical model and simulate what a given configuration would measure. Essentially, we subsample the full model circulation at a sampling rate that would be achievable from measurements in the real ocean. While such a test is inherently limited by the shortcomings of the underlying model, it does have the advantage that we can test different configurations and compare them directly against the full model solution. Here, we use a model at eddy-permitting resolution (ORCA025 with 0.25° resolution, Barnier et al. 2006).

Specifically, we investigate two options: (1) an observing system based on new measurements closing Line W zonally along 32°N, which is methodologically a transfer of RAPID/MOCHA to 32°N, (2) an observing system closing Line W with existing instruments of RAPID/MOCHA at 26°N and moorings next to Bermuda (Hydrostation 'S' and Bermuda Atlantic Time-Series Study; Phillips and Joyce (2007)). These tests do not imply that a potential observing system based on Line W would be the only option, but building on an existing observing array ideally allows an AMOC estimate for economizing time, costs, and maintenance cruises. With the present study, we aim to test what would be required to estimate the full AMOC based on the Line W boundary array.

This study is organized as follows. Section 2 provides technical details about the employed numerical model output and the method. Section 3 presents an analysis of the capability of using different sections to monitor the AMOC as well as array simulations based on 26°N, 32°N, and Line W. Sections 4 and 5 contain a discussion and conclusions, respectively.

2 Methods and model

2.1 Simulated sections

We simulate observing systems at three sections: one based on the existing 26°N RAPID/MOCHA array, one based on the existing Line W boundary current array, and one where RAPID and Line W are combined (Fig. 1, Table 1). The section 26°N consists of three parts: (1) The WBC, which is confined to Florida Straits between Florida and the Bahamas, and which has high northward velocities with maximum amplitudes of 1.8 m/s, (2) the mid-ocean area west of the westernmost MAR mooring of RAPID/MOCHA ($26°N_{West}$), and (3) the mid-ocean area east of the westernmost MAR mooring of RAPID/MOCHA ($26°N_{East}$, c.f. Fig. 1).

For the two sections based on Line W, the WBC lies between New England and Bermuda, and is no longer geographically confined. The Line W DWBC array is located at the continental slope south of New England and does not cover the surface flow. Here, we first assume the WBC transport to be known for the basin-wide observing system (as for the 26°N RAPID array), and then test how the existing observations at Line W must be extended to capture the total transport across the western boundary. After that, we test potential observing systems based on the extended Line W array.

For the potential observing systems, Line W is first closed zonally across the basin, i.e., a mid-ocean part between Bermuda and West Africa across 32°N is estimated (Line W-32°N). Second, Line W is combined with $26°N_{East}$ of RAPID and is closed by the section B-MAR between Bermuda and the westernmost MAR mooring of RAPID/MOCHA (Line W-B-RAPID, c.f. Fig. 1). Note that Bermuda in the model is represented by a seamount ending 380 m below the surface. The entire WBC and DWBC are contained between the coast and the Bermuda Rise, with WBC and DWBC lying side by side (Fig. 2b, c).

2.2 Model and data set

The data used for the observing system simulations stem from the global eddy-permitting ORCA025 model configuration of the DRAKKAR project (Barnier et al. 2006; The DRAKKAR Group 2006; and Madec 2008). The model consists of an ocean circulation model (based on OPA9 code) coupled to the LIM2 sea-ice model (Goosse and Fichefet 1999). The model grid (Arakawa C grid) is centered at tracer points and has a resolution of 1/4°. The actual resolution used in our observing system simulations is 24.9 km at 26°N increasing to 20.9 km at 41°N (northern area of LineW). The vertical grid consists of 46 non-equidistant vertical levels, ranging from 6 m at the surface to 250 m

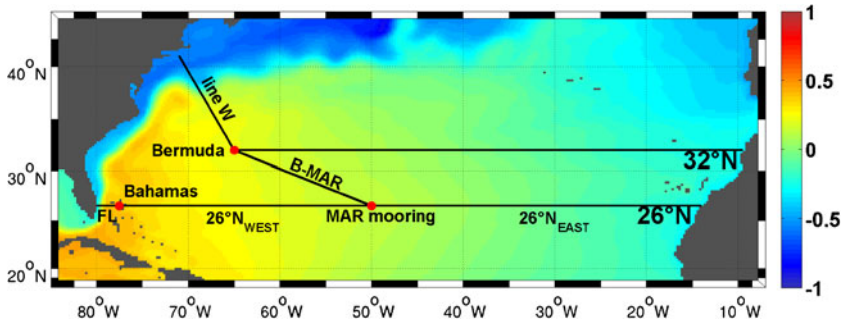

Fig. 1 Mean SSH in meters (1998–2007) from ORCA025 and map of the investigated transects at 26°N, LineW-B-RAPID, and LineW-32°N with its different sections. Line W extending from the shelf of New England to Bermuda, B-MAR section between Bermuda and the western MAR mooring of RAPID/MOCHA, and the 26°N$_{West}$ and 26°N$_{East}$ sections west and east of the westernmost MAR mooring of RAPID/MOCHA

in bottom layers. In addition, partial cells are used in the vertical at the bottom for a better representation of small topographic slopes (Barnier et al. 2006).

In the present study, we use the model output from an ORCA025 configuration forced by a global climatology based on NCEP reanalysis data (Large and Yeager 2009). We use 16 years of model data with 5-day means (1992–2007). If not remarked differently in the figure caption, the time series shown in this paper are smoothed with a 30-day running mean in order to reduce short time and high frequent signal contributions which are more likely to be ageostrophic. For every investigated section, temperature, salinity, zonal and meridional velocities, and wind stress are used. Temperature and salinity are interpolated linearly to meridional velocity points of the model grid. Afterwards, in situ density is calculated using the Jackett and McDougall (1995) equation of state for seawater following the model.

2.3 Method

Decomposition To estimate the full AMOC, we decompose it into individually observable components. The decomposition is similar to what is used to construct the 26°N RAPID AMOC estimate (c.f. Kanzow et al. 2007), which is conceptually based on the decomposition of the AMOC by Lee and Marotzke (1998) and Marotzke et al. (1999). This decomposition was also tested in model design studies by Hirschi et al. (2003) and Baehr et al. (2004). We briefly describe the method here, mostly focussing on its adaptation to the present study. The full model AMOC at a specific latitude is given by

$$\psi(z) = \int_{z}^{0} \int_{x_W}^{x_E} v(x,z)\, dx\, dz, \tag{1}$$

where x_W and x_E are the western and eastern limits of the basin, respectively, v the meridional velocity, and H the maximum depth of the transect. In our observing system simulations, we compare the full modelled AMOC against a reconstructed AMOC ψ_{rec}, which is the sum of a WBC component ψ_{wbc}, a mid-ocean component ψ_{tw} derived from thermal wind and an Ekman component ψ_{ek}:

$$\psi_{rec}(z) \approx \psi_{\mathrm{wbc}}(z) + \psi_{tw}(z) + \psi_{ek}(z). \tag{2}$$

We use the following convention for the individual components of the AMOC to distinguish between the sections: ψ^{26} for 26°N RAPID/MOCHA, $\psi^{w/32}$ for Line W-32°N, and $\psi^{w/26}$ for Line W-B-RAPID.

To ensure mass balance across the zonal transect, we introduce a spatially, but not temporally constant mass balance correction. We apply this correction separately to the Ekman transport and the sum of $\psi_{\mathrm{wbc}} + \psi_{tw}$. Essentially, we assume that the Ekman transport is balanced by a zonally and vertically constant (barotropic) flow. The Ekman

Table 1 Summary of sections in the present study

Section Name	WBC	Mid-Ocean
26°N	Florida Straits	26°N$_{West}$+ 26°N$_{East}$ (9 RAPID moorings)
Line W-32°N	Line W	32°N (no observational equivalent exists)
Line W-B-RAPID	Line W	B-MAR and 26°N$_{East}$ (Hydrostation 'S'+5 RAPID moorings)

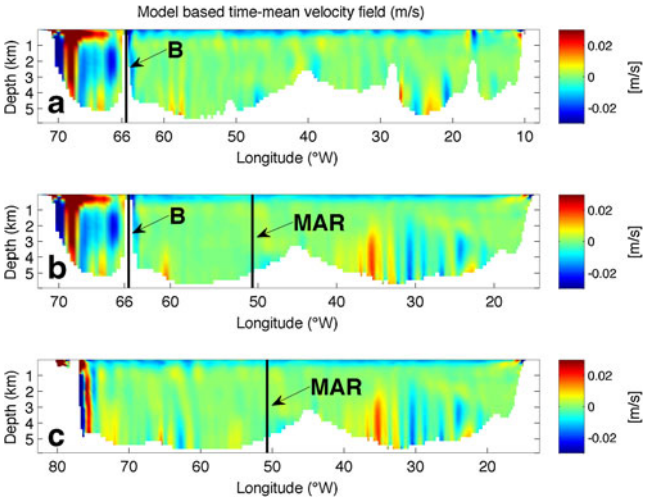

Fig. 2 Vertical transects of transects at **a** LineW-32°N, **b** LineW-B-RAPID, and **c** 26°N, showing the topography and model-based time-mean velocity fields of the transects, velocities in meters per second. The *arrows labeled with B* in **a** and **b** indicate the Bermuda Rise in the model, the *arrows labeled with MAR* in **b** and **c** indicate the western MAR mooring of the RAPID array

transport is corrected following Lee and Marotzke (1998) and Hirschi et al. (2003). We further assume that the interior transport (ψ_{tw}) and the western boundary current balance each other. Specifically, we calculate a correction velocity ($\hat{v}_{tw}$) as in Hirschi et al. (2003):

$$\hat{v}_{tw} = \frac{\psi_{\mathrm{wbc}}(-H) + \psi_{tw}(-H)}{A}, \tag{3}$$

where the transport imbalance of the zonal section $\psi_{\mathrm{wbc}}(-H) + \psi_{tw}(-H)$ is divided by the section area A. Mimicking a realistic observing system, we apply the correction velocity only to ψ_{tw}:

$$\hat{\psi}_{tw}(z') = \int_{x_\mathrm{W}}^{x_\mathrm{E}} \int_{-H}^{z'} (v_{tw} - \hat{v}_{tw})\, dz\, dx. \tag{4}$$

The mass balance corrected reconstruction of the AMOC is then

$$\hat{\psi}_{rec}(z) = \psi_{\mathrm{wbc}}(z) + \hat{\psi}_{tw}(z) + \hat{\psi}_{ek}(z). \tag{5}$$

Mid-Ocean component The calculation of the mid-ocean component is based on the thermal wind equation ($f\frac{\partial v}{\partial z} = -\frac{g}{\rho_0}\frac{\partial \rho}{\partial x}$, where f is the Coriolis parameter, g the gravitational acceleration, and ρ_0 a reference density) using densities at the eastern and western boundaries of the basin, from which the meridional velocity can be calculated, to reconstruct a meridional streamfunction $\psi_{tw}(z)$ (as in Hirschi et al. 2003):

$$\psi_{tw}(z') = \int_{x_\mathrm{W}}^{x_\mathrm{E}} \int_{-H}^{z'} v_{tw}\, dz\, dx. \tag{6}$$

This streamfunction is corrected in order to hold mass balance as shown above. At 26°N and 32°N, the mid-ocean transport is purely meridional, whereas the transport across the section B-MAR of Line W-B-RAPID is rotated in cross-sectional direction. To "measure" the density gradient for the meridional velocity, we place several density profiles across the basin, which represent moorings deployed in the ocean.

Western boundary current In our simulations, we first assume the WBC component ψ_{wbc} to be completely known, and therefore calculate it directly from the model velocity field. At 26°N, we calculate ψ_{wbc}^{26} from the meridional model velocity field in the Florida Straits. At Line W-32°N ($\psi_{\mathrm{wbc}}^{w/32}$) and at Line W-B-RAPID ($\psi_{\mathrm{wbc}}^{w/26}$), we calculate the WBC component from the meridional and zonal velocity field and rotate it to ensure a cross-sectional transport which is perpendicular to the used configuration representing Line W.

Since the assumption of a completely known velocity field at Line W is not justifiable from observations, we subsequently deploy the Line W array as realistically as possible by using density profiles, as well as direct velocity measurements at three places. To obtain the total transport between New England and Bermuda, we extend the existing Line W array to the sea surface and place two additional moorings at the Bermuda Rise. The full WBC transport is calculated from the following components:

$$\psi_{\mathrm{wbc}}^{w/32} = \psi_{\mathrm{LineW}} + \psi_{\mathrm{LineW\_extension}} + \psi_{\mathrm{LineW\_east}}, \tag{7}$$

where ψ_{LineW} is the transport "measured" by the Line W array, $\psi_{\mathrm{LineW\_extension}}$ represents the extension of the Line W array to the sea surface, and $\psi_{\mathrm{LineW\_east}}$ is the residual flow of the western boundary based on the easternmost profile of the Line W array and two additional density profiles at Bermuda. To capture ψ_{LineW} and $\psi_{\mathrm{LineW\_extension}}$, we use density profiles for thermal wind balance and in addition to direct velocity observations. To ensure mass balance, we apply the mass balance correction to both the mid-ocean transport and the contribution obtained from Line W.

Ekman component We calculate the Ekman transport based on the meridional wind stress, which is assumed to be known from observations. Further details about the calculation of the Ekman component and its implementation in the

simulated observing system can be found in Hirschi et al. (2003) and Baehr et al. (2004). For the Line W and B-MAR, we rotate the Ekman transport in cross-sectional direction from the meridional and zonal Ekman transport.

3 Results

3.1 Analysis of the modeled AMOC variability

Modelled AMOC variability vs. RAPID/MOCHA at 26°N Before we simulate AMOC observing systems, we compare the modeled AMOC to the observations from the RAPID/MOCHA array at 26°N to assess whether the model can represent the observed AMOC variability. For the overlapping period of the array observations and the ORCA025 model simulation (April 2004–December 2008), we compare monthly mean values of the AMOC and its components (Fig. 3). The magnitude and variability of the total model AMOC at 26°N ($\psi^{26} = 17.8 \pm 2.7$ Sv) is in the same order of the RAPID/MOCHA AMOC (18.7 ± 3.9 Sv), the correlation coefficient between them is about 0.64.

The large coherence of the AMOC of the model and RAPID/MOCHA results from the dominance of the wind forcing on seasonal to interannual timescales (Biastoch et al. 2008), which is highly correlated between the model and RAPID/MOCHA, although the strong influence of the Florida current which is not reproduced in the model (RMSE = 6.2 Sv) controls the large RMSE between the

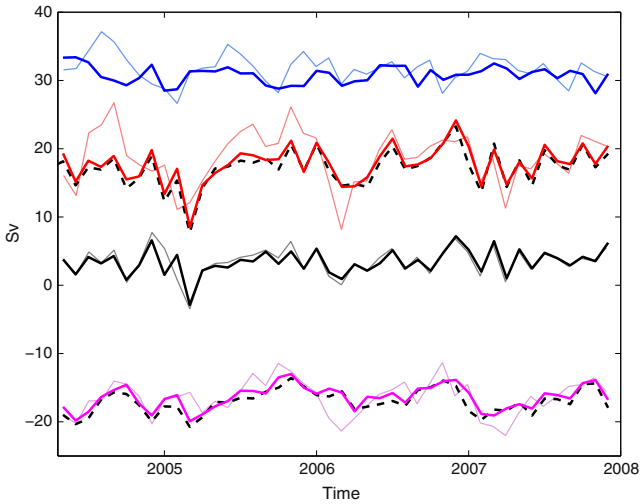

Fig. 3 26°N: modelled transports (*thick lines*) and transports of RAPID/MOCHA (*thin lines*) between April 2004 and December 2007. Western boundary current component (*blue*), AMOC (*red*), mid-ocean transport (*magenta*), and Ekman component (*black*). The *dashed lines* show the reconstructed mid-ocean transport and reconstructed AMOC in the model based on thermal wind balance. The description of the dashed lines can be found in Section 3.2(i).

AMOC of the model and RAPID/MOCHA (6 Sv). The mid-ocean contribution in the model is calculated from the residual of $\psi^{26}_{mo} = \psi^{26} - \psi^{26}_{\mathrm{wbc}} - \psi^{26}_{ek}$ (-16.4 ± 1.7 Sv), and is in the order of the mid-ocean component of RAPID/MOCHA (-16.5 ± 2.6 Sv). They have a correlation coefficient of 0.67 and a RMSE of 0.3 Sv showing that the model realistically represents the observed mid-ocean variability. Overall, the modeled AMOC and its components largely reproduce the RAPID/MOCHA estimates in their time-mean value and temporal variability, with the exception of the Florida Current whose strength is generally reproduced by the model, but the variability differs in detail.

Modeled AMOC variability of the simulated sections We now turn to the three sections 26°N, Line W-32°N, and Line W-B-RAPID and analyze the variability of the AMOC and its components, directly computed from the model velocity field in the top 1,000 m.

At 26°N, the AMOC is $\psi^{26} = 17.6 \pm 2.7$ Sv (Fig. 4). For the Line W-based sections, the AMOC is weaker than at 26°N, because of the compensation of the northward flowing WBC by the southward flowing DWBC ($\psi^{w/32} = 11.8 \pm 5.6$ Sv at Line-32°N, and $\psi^{w/26} = 12.5 \pm 6.0$ Sv at Line W-B-RAPID, Fig. 4). In the model, WBC and DWBC are lying side-by-side below 300 m depth at the western edge of Line W, in contrast to 26°N where the DWBC sits below the maximum AMOC at 1,000 m. Similar observations of the WBC and the DWBC flowing side-by-side at Line W were obtained by Toole et al. (2011). With the WBC no longer confined to a strait, the AMOC shows a larger STD for the Line W-based sections than at 26°N.

Comparing the two Line W-based sections with the section 26°N, no significant correlation can be found between 26°N and the Line W-based AMOC ($\psi^{w/32}$ and $\psi^{w/26}$), the mid-ocean ($\psi^{w/32}_{mo}$ and $\psi^{w/26}_{mo}$), and WBC contribution ($\psi^{w/32}_{\mathrm{wbc}}$ and $\psi^{w/26}_{\mathrm{wbc}}$) over the 16 years of model data analyzed here. Including also the Antilles current, flowing east of the Bahamas, into the WBC at 26°N reveals no significant relation to the Line W WBC. Comparing the two Line W-based lines with each other does show a significant correlation for the AMOC (0.95). This is only partly because the two sections are based on the same WBC component as the two mid-ocean components $\psi^{w/32}_{mo}$ and $\psi^{w/26}_{mo}$ are also significantly correlated (0.92, Fig. 4), suggesting that most of the variability of the mid-ocean originates from the western part of the basin. Thus, an observing system combining Line W with either observations across 32°N or RAPID observations has the potential to deliver an estimate of the mid-ocean transport independent of the RAPID-26°N estimate.

The variability between the RAPID-26°N section and the Line W-based sections shows little coherence on monthly timescales supporting Bingham et al. (2008). The wind

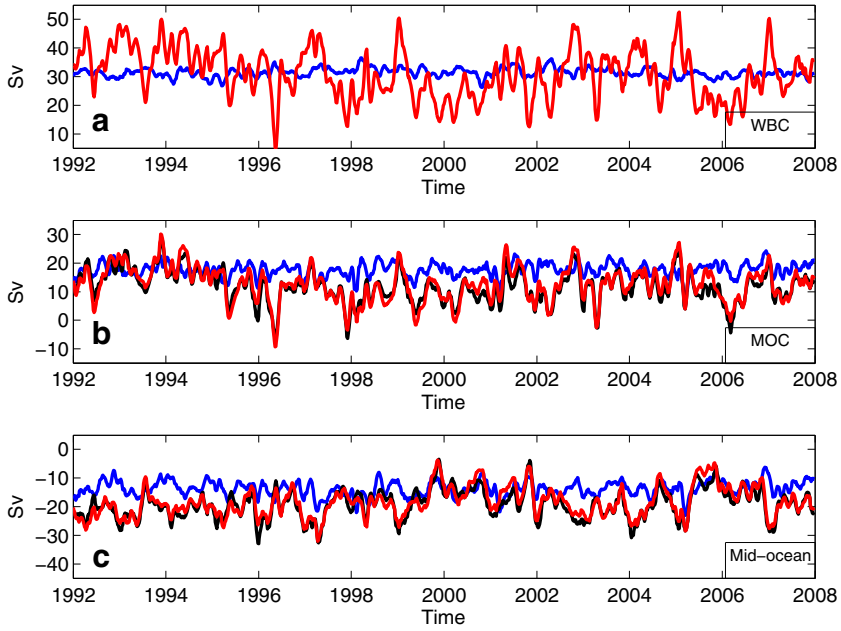

Fig. 4 Contributions to the AMOC and their variability at 26°N (*blue*), Line W-B-RAPID (*black*), and Line W-32°N (*red*): **a** WBC component, **b** AMOC, and **c** mid-ocean component

forcing clearly dominates the variability of the AMOC at the investigated sections on seasonal to interannual timescales. In the model, Line W is situated in a region where the Gulf Stream detaches from the coast, begins to meander, and forms eddies. These eddies spread predominantly eastward leading to a strongly increased variability of the Line W transport and introduce additional noise into the "observations". Kanzow et al. (2009) noted that the across-section translation of an eddy would influence the pressure gradients when passing an endpoint of trans-basin observing systems, as the northern/central part of Line W. Furthermore, the model reveals an unfortunate misrepresentation in the area of Line W in the model. In this region, we find a pronounced standing eddy pattern which is not present in real observations but a common problem in ocean models, even at higher resolution (Barnier et al. 2006). Owing to advanced numerics and the partial cells approach, the transport of this "unrealistic Hatteras eddy" is significantly reduced but still existent (Barnier et al. 2006). The presence of the standing eddy leads to increased variability of the transport and to non-geostrophic contributions in the velocity field. This can also be seen in the Eulerian overturning streamfunction which we consider in this study or the temporal evolution and STD of the barotropic streamfunction at the western boundary (not shown).

The increased variability between 34°N to 40°N can also be seen in zonal transects where the STD of the AMOC is increased to about 3.5 Sv, albeit it is less intensified than at Line W. But the transport measured at Line W includes a strong influence of the zonal flow, such that the relation between latitudes of 34°N to 40°N and Line W is generally lower than between pure zonal transects.

In order to understand whether the increased variability stems from the standing eddy or is generally found for angled sections, we test an arbitrary section south of Line W and outside of the standing eddy pattern (zonally across about 31°N, angled line at western boundary from 31°N-35°N, not shown). In the angled section, we find a mean AMOC of 14.9 Sv with a standard deviation of 2.9 Sv. The standard deviation and the variability is comparable to pure zonal sections, which further suggests that the standing eddy causes the increased variability found at Line W and we cannot generally assume that angled sections project more variability on the AMOC.

In the present model, the variability of the 26°N AMOC is dominated by the mid-ocean component (correlation coefficient of 0.81 between mid-ocean and AMOC, compared to 0.15 between WBC and AMOC). In contrast, the variability of the Line W-based AMOC is dominated by the WBC variability (correlation coefficient of 0.84 between Line W and AMOC at Line W-32°N, correlation coefficient of 0.82 between Line W and AMOC at Line W-B-RAPID), which confirms that an AMOC reconstruction based on Line W appears to be largely 26°N-independent. This strong dependence on the western boundary variability demands an individual analysis of the representativeness of the Line W observations, which we conduct in Section 3.2(5).

3.2 Simulation of potential observing systems

Having analyzed the variability in the model velocity field, we now simulate an AMOC observing system by subsampling the model output. Therefore, we deploy several

density profiles across the basin to "measure" the thermal wind component of the total AMOC (Eq. 5) in the model.

(1) *26°N – RAPID/MOCHA* First, we simulate the existing RAPID/MOCHA array at 26°N. We deploy nine density profiles across the basin at 26°N in the model, mimicking the deployed moorings of RAPID/MOCHA. At the given model resolution, the RAPID array can be conceptually represented with dense coverage at the eastern and western boundary and moorings at the Mid-Atlantic Ridge. But the resolution is too coarse to resolve the specific placement of individual moorings within the boundary arrays. Similarly to Hirschi et al. (2003), we use four density profiles placed at the western boundary, two profiles at both sides of the MAR, and three profiles at the eastern boundary of the mid-ocean region. At 26°N, the WBC is geographically separated from the mid-ocean region by the Bahamas, and we assume it to be completely known.

At 26°N, the reconstructed mid-ocean transport ψ_{tw}^{26} (-17.0 $\pm$ 1.7 Sv) is slightly larger than the modeled one (-16.4 $\pm$ 1.7 Sv) given by $\psi^{26} - \psi_{\mathrm{wbc}}^{26} - \psi_{ek}^{26}$, but reproduces the variability well (correlation coefficient of 0.91 between reconstructed and modeled mid-ocean transport, Fig. 3). The total reconstructed AMOC ψ_{rec}^{26} (17.2 $\pm$ 2.8 Sv) therefore slightly underestimates the modeled AMOC ψ^{26} (17.8 $\pm$ 2.7 Sv), but captures the variability on monthly scales indicated by a correlation coefficient of 0.97.

(2) *Line W-32°N – from the maximum number of 222 profiles to 4 profiles* Second, we simulate an observing system closing Line W by a zonal transect at 32°N. To reconstruct $\psi_{tw}^{w/32}$, we place several moorings between Bermuda and the coast of West Africa along 32°N. Methodologically, this represents a direct transfer of RAPID/MOCHA to 32°N by splitting up the AMOC into a WBC component, a mid-ocean component, and an Ekman component. Placing a density profile at every grid cell along 32°N (Fig. 5a), i.e., simulating the use of all possible density information, reveals the highest order of information gained from reconstructing the mid-ocean component.

The modeled AMOC has a time mean value of 11.8 Sv with a STD of 5.6 Sv. The reconstruction based on all possible density information slightly underestimates the AMOC with a time mean value of 11.1 Sv and a STD of 5.5 Sv, where the modeled variability is very closely captured (not shown). This is supported by a small RMSE of 1 Sv. Both, the modeled AMOC and its reconstruction reveal a high variability, though this large variability originates from the WBC component at Line W (Fig. 3). The vertical profile reveals that the AMOC below 2,000 m is systematically underestimated (Fig. 5b), which is mostly due to an underestimation of bottom velocities occurring when the flow hits topography (not shown).

When the number of profiles is reduced to a RAPID-like array with 10 profiles, the RMSE between AMOC and its reconstruction increases to 1.6 Sv (Fig. 5c, e, f, compared to 1 Sv for all density information). The vertical profile of the AMOC minus its reconstruction (Fig. 5c) reveals an improved estimate, while the deep return flow is slightly underestimated below 3,000 m (Fig. 5f). Note that this improved representation of the deep return flow is merely the consequence of a reduced error accumulation when reducing the number of profiles from 222 to 10.

To assess the relevance of the mid-ocean component to the total AMOC, we test a minimalistic observing system setup using only four profiles, two at each side of the basin (two westernmost and two easternmost profiles in Fig. 5a). Somewhat surprisingly, the reduction to four profiles leads to no significant decrease of quality of the reconstruction (Fig. 5d). The modeled AMOC is captured remarkably well in its strength and variability with bias of 0.02 Sv and a correlation coefficient of 0.99. The RMSE is with 1 Sv only slightly larger than for the maximum number of profiles. Also, the reduction to four profiles leads to comparably little misestimation of deep return flow (Fig. 5d), though no density information below 2,200 m enter the calculation in the interior. This appears to be a fortunate compensation of errors, where overestimates and underestimates cancel each other in the large bottom triangles.

(3) *Line W-32°N with a time-mean WBC* Since, as the previous results confirm, most of the variability of the AMOC originates from the WBC component across Line W, we now analyze the mid-ocean component separately. To allow for a comparison with previous results, we reconstruct the full AMOC but hold the WBC temporally constant. The resulting AMOC based on the full density field still shows a STD of 1.8 Sv (Fig. 6, compared to a STD of 5.5 Sv for the full AMOC). The reconstructed AMOC based on the maximum number of profiles has a STD of 1.8 Sv, as well. The RMSE between the full modelled AMOC and the reconstruction is 5.3 Sv and shows again the high impact of the WBC variability on the total AMOC, whereas the RMSE between the modelled AMOC with temporally constant WBC and its reconstruction is 1 Sv (Fig. 6a, b). Reducing the number of profiles to 10 increases the RMSE to 1.6 Sv, mostly from a slight underestimation in the variability (Fig. 6c, d). Reducing the number of profiles to four (two at the western boundary and two at the eastern boundary), the RMSE between the modelled AMOC and its reconstruction yields 1.1 Sv (Fig. 6e, f). Holding further the eastern boundary profiles constant to its mean value, and only allowing temporal variations of the two westernmost profiles at 32°N, significantly reduces the variability of the reconstructed AMOC (RMSE increases to 1.4 Sv), while the errors in the vertical profile are largely unchanged

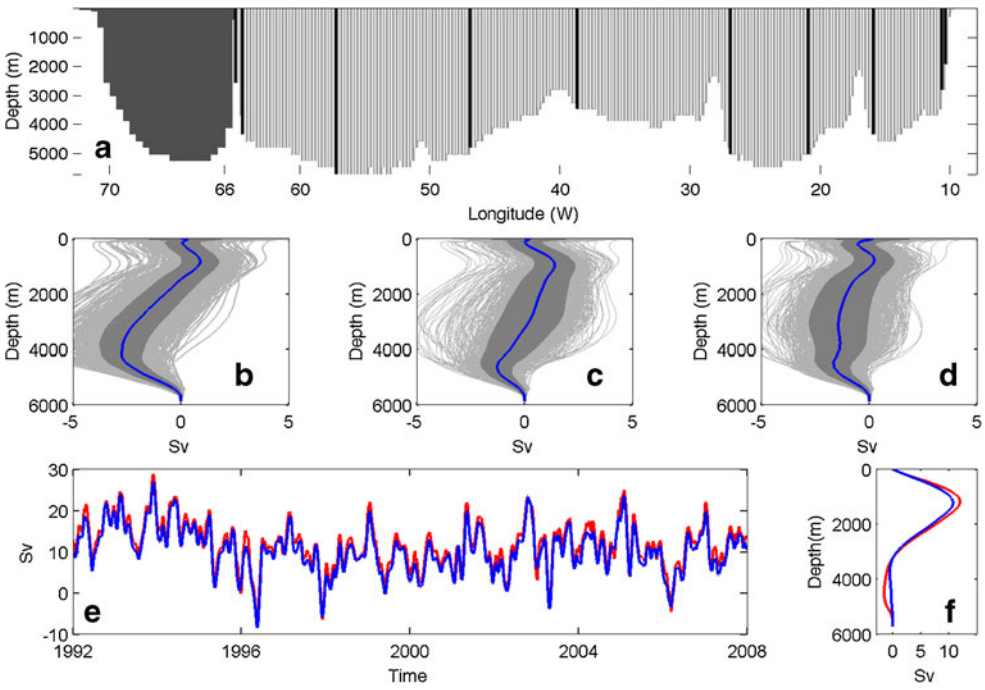

Fig. 5 AMOC at LineW- 32°N and its estimate based on density profiles at every grid cell: **a** Topography with placed density profiles. Maximum number of 222 profiles in *white*. Reduced number of density profiles in *black*. *Dark gray area* shows the transect of Line W where the velocity field is assumed to be completely known. **b**–**d** Difference of the AMOC and its reconstruction based on 222 density profiles (**b**), 10 density profiles (**c**), and 2 profiles at the western and 2 profiles at the eastern boundary (**d**). Time mean in *blue*, every time step in *gray*, and standard deviation in *dark gray*. **e** Time series of the AMOC (*red*) and its reconstruction based on 10 profiles (*blue*) at 1,000 m. **f** Vertical time mean profile of the AMOC (*red*) and its reconstruction (*blue*)

(Fig. 6g, h). These tests indicate that although the total AMOC is dominated by the WBC contribution, the reconstruction is sensitive to the number and location of profiles chosen. In particular, both, the western and eastern boundary contribute to the variability. As no eastern boundary moorings exist presently at 32°N in the real ocean, we now turn to testing to close Line W further south relying on existing observations.

(4) *Testing a realistic Line W western boundary array* Having tested possible observing strategies for the interior transport, we now analyze the influence of the WBC variability separately. We therefore construct a hypothetical observing system where the AMOC is based entirely on the Line W variability. Such a setup would not use any density information from the mid-ocean, but only a compensation of the western boundary. An AMOC based on such an observing system captures a dominant part of the total variability (correlation of 0.8, not shown).

The assumption that the transport across the complete western boundary is measured perfectly is not justified at Line W, since the existing moorings cover mainly the

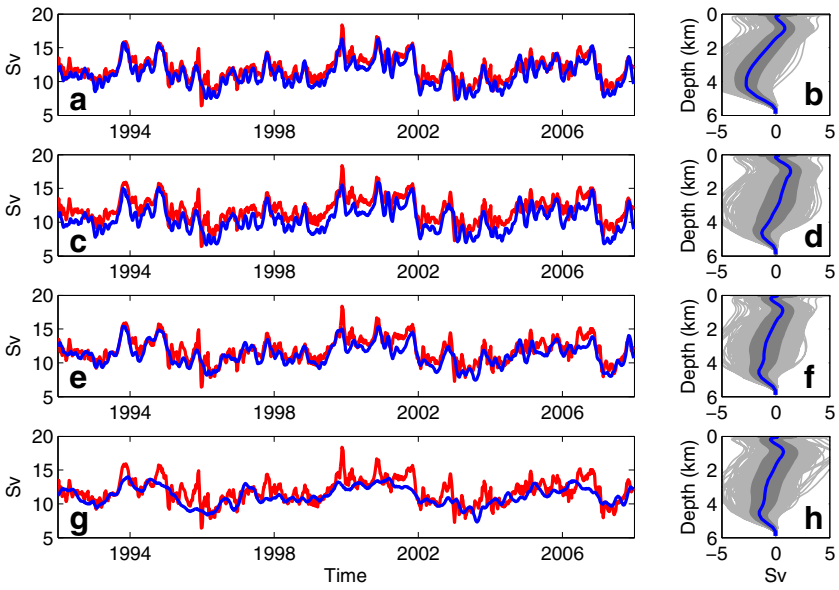

Fig. 6 Line W-32°N with time-mean Line W transport: Time series of the AMOC based on a time-mean WBC component (*red*) and its estimates based on a time-mean WBC component (*blue*) using **a** the full number of 222 profiles, **c** 10 profiles, **e** 2 profiles at the western and 2 profiles at the eastern boundary, and **g** 2 profiles at the western and 2 profiles at the eastern boundary with constant eastern boundary profiles. **b**,**d**,**f** and **h** Vertical profile of the difference between the AMOC and its reconstruction showing the absolute error (*light gray*), time-mean (*blue*), and STD (*dark gray*)

continental slope to observe the DWBC. The determination of the total transport at the western boundary, which includes the WBC and the DWBC, is not yet realized within the Line W DWBC array. Therefore, we test now an observing system simulating the WBC measurements with a combination of existing observations at Line W and an extension to Bermuda.

We assume the total WBC transport can be composed from three sets of moorings (Fig. 7): (1) the existing Line W similar to its presently deployed setup in the Atlantic which delivers temperature, salinity measurements, and direct current meter measurements to measure the DWBC (ψ_{LineW}, white lines in Fig. 7) but omitting the surface flow (Toole et al. 2011), (2) an extension of Line W to the surface ($\psi_{\mathrm{LineW\_extension}}$, black box at the surface in Fig. 7), and (3) additional moorings to cover the basin to the Bermuda Rise ($\psi_{\mathrm{LineW\_east}}$, two black moorings at Bermuda in Fig. 7). The moorings (2) and (3) are presently not deployed in the Atlantic, but these observations are necessary to determine the total flow ($\psi_{\mathrm{wbc}}^{w/32}$) between New England and Bermuda.

For the relative velocities computed from thermal wind balance at Line W, a reference level is assumed at about 1,000 m deep.

The Line W contribution ψ_{LineW} to the total WBC mostly consists of the deep flow (Fig. 8a, b). The transport of the upper 2,000 m is captured almost perfectly (correlation of 0.99, RMSE of 0.1 Sv). But the strong surface velocities of the WBC (see Fig. 2), which account for a large amount of the magnitude and variability of the western boundary transport (Fig. 8c, d) must be covered by the extension of Line W array to the surface by (2).

The transport $\psi_{\mathrm{LineW\_extension}}$ is also measured accurately (correlation coefficient of 0.99, RMSE of 2 Sv). In addition, the missing (geostrophic) contribution between the easternmost Line W mooring and the western boundary moorings near Bermuda (Fig. 8e, f) must be obtained by (3) for the total WBC transport from the thermal wind balance (Fig. 8g, h). Using a setup which is close to the real Line W array, we obtain a reasonable correlation (0.97), but a large RMSE (5.2 Sv).

These differences stem from the presence of the unrealistic Hatteras eddy. For test purposes, we add direct velocity measurements to this area and extend the Line W array to the east (red moorings in Fig. 7 (iv)), which yields a better representation of the transport between Line W and Bermuda (Fig. 8e, f, correlation coefficient of 0.99, RMSE of 2.5 Sv). Given that the standing eddy is a known model deficit (Barnier et al. 2006), the suggested Line W extension is constrained to additional surface observations (2) only.

The total transport $\psi_{\mathrm{wbc}}^{w/32}$ is largely reproduced (correlation coefficient of 0.89, RMSE of 6.2 Sv), although the measurements overestimate the model transport directly calculated from the velocity field, and the pronounced peaks cannot be reproduced. Deviations in the lower layers occur as the method does not capture bottom velocities, and the mass-balance correction in our simulations is applied to both Line W and mid-ocean. Extending Line W to the east to capture the standing eddy leads to a better representation of the western boundary transport (Fig. 8g, h, correlation coefficient of 0.97 and RMSE of 3.9 Sv).

In summary, the total WBC can be measured based on Line W, its extension to the sea surface and to the east and

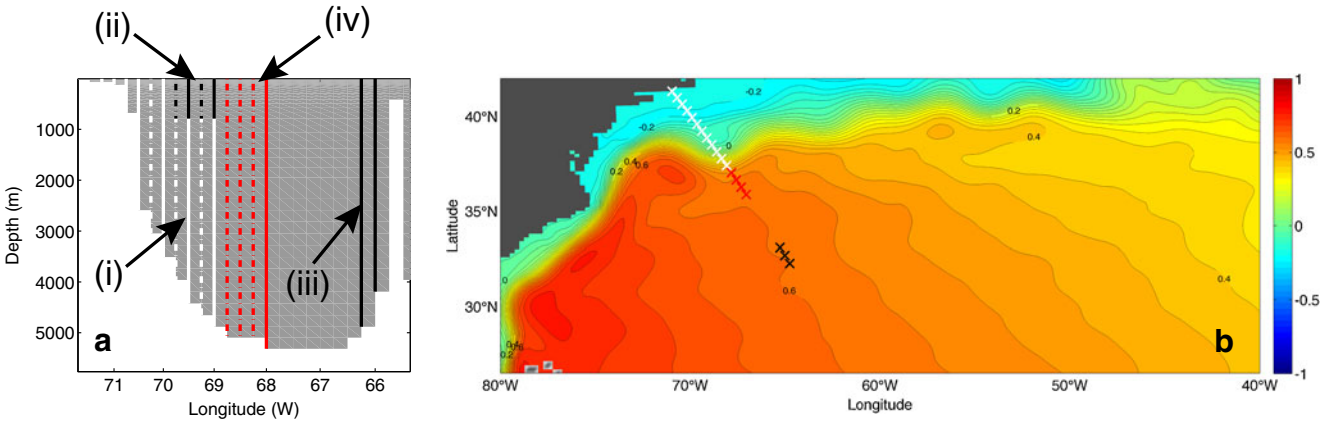

Fig. 7 **a** Configuration of Line W in the simulated observing system. *White lines (i)* represent existing observations at Line W where the *solid lines* are used to measure T and S and the *dashed lines* represent direct measurements of velocities. *Black lines (ii)* represent how the existing Line W is extended to the surface. *Black lines (iii)* represent needed moorings at Bermuda to capture the WBC in the model and to close the observing system. *Red lines (iv)* show how Line W is extended in the model to the east by T and S profiles and direct velocity measurements to cover and capture the unrealistic standing eddy which is existent in the model. **b** Mean sea surface height (1998–2007) from ORCA025 showing the "unrealistic Hatteras eddy" at Line W with the position of existing Line W moorings (*white*), of the extension to the east (*red*) and of the moorings at Bermuda (*black*). Contour interval is 4 cm

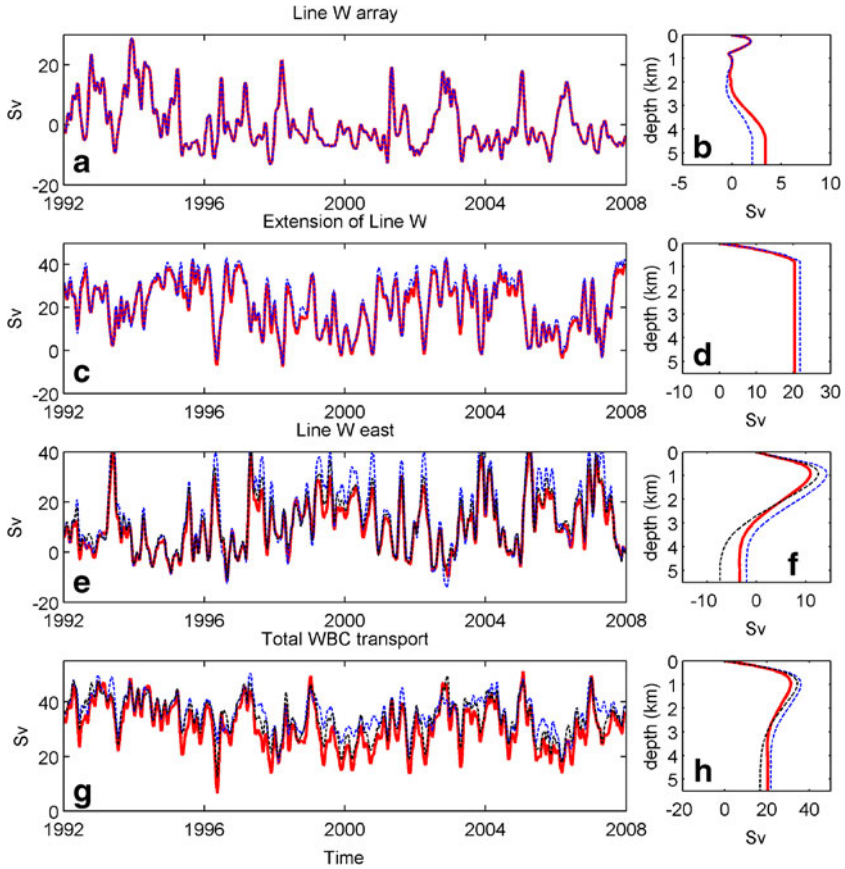

Fig. 8 Transport across Line W array and the components extending Line W, which are used to measure the total WBC. Model transport: *solid red lines*, reconstruction from direct velocities and thermal wind: *dashed blue lines*, reconstruction from direct velocities and thermal wind where Line W is extended to the east to cover the standing eddy: *dashed black lines*. **a** Line W array (*(i)* in Fig. 7), mimicking the array in the Atlantic. **b** Corresponding vertical profile of the volume transport. **c** Extension of the Line W array to the sea surface (*(ii)* in Fig. 7). **d** Corresponding vertical profile. **e** Additional measurements of the eastern part of the WBC between the easternmost mooring of the Line W array mimicking the array and moorings at the Bermuda Rise (*(iii)* in Fig. 7, *dashed blue*) , and of the eastward extension of Line W to cover the standing eddy (*(iv)* in Fig. 7) and moorings at Bermuda (*dashed black*). **f** Corresponding vertical profile. **g** Total transport between New England and Bermuda that is the sum of the components in **a**–**e**. Colors as in **e**. **h** Corresponding vertical profile

two additional moorings at the Bermuda Rise. Using such a setup for a hypothetical AMOC reconstruction, assuming only a compensation of the WBC in the mid-ocean, the variability of the measured transport across Line W still represents the AMOC variability with a correlation coefficient of about 0.7.

(5) *Line W-32°N based on a realistic Line W western boundary array* Now, we combine our extended Line W array with 10 profiles placed across the basin at 32°N (see Section 3.2(2)). Since the extended setup of Line W overestimates the total WBC transport, the reconstruction (mean of 14.8 Sv) overestimates the AMOC by 3 Sv (Fig. 9b). Further, the decreased variability of the reconstructed AMOC (STD of 4.8 Sv) reflects the variability obtained from the western boundary. This is also mirrored by an RMSE of 4.3 Sv. The vertical profile reveals that the general structure can be obtained from the observing system, though the reconstruction overestimates the AMOC in all layers (Fig. 9c). The Hovmoeller diagram showing the difference between AMOC and its reconstruction also indicates that the AMOC is largely overestimated by its reconstruction through all layers (Fig. 9d). Nevertheless, a correlation coefficient of 0.84 confirms a proper reconstruction of the AMOC variability based on observations at Line W, Bermuda, and 32°N. Including direct velocity measurements of the standing eddy into the reconstruction (correlation coefficient of 0.88, RMSE of 3.6 Sv) yields a slightly better estimate of the AMOC, but the maximum AMOC is still overestimated resulting from the overestimated WBC (Fig. 9b).

(6) *Line W-B-RAPID – fully known WBC and sensitivity to the number of profiles* As an alternative option to close

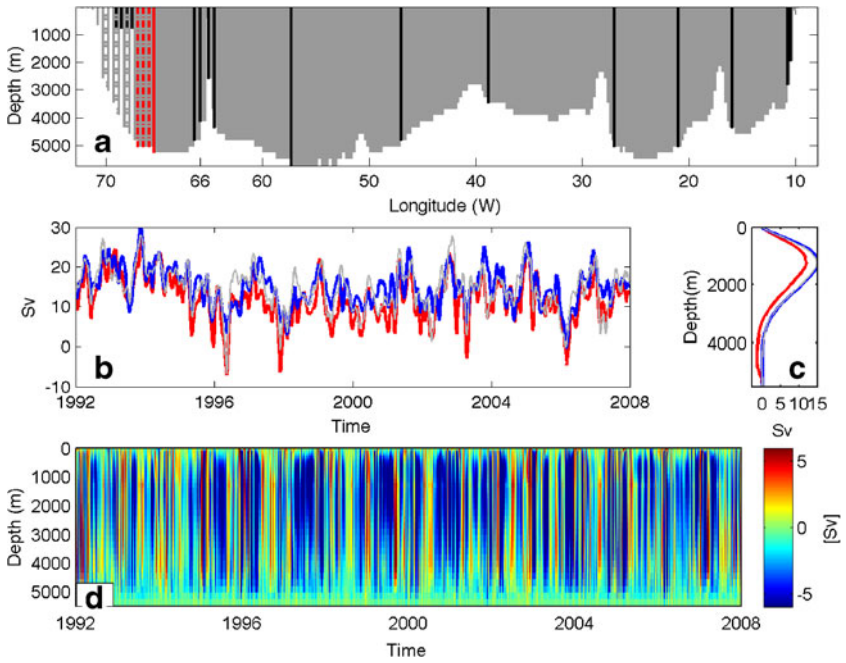

Fig. 9 AMOC at LineW-32°N and its estimate based on measurements at Line W and in the mid-ocean: **a** Topography with placed density profiles. *White lines* represent existing observations at Line W, where the *solid lines* are used to measure T and S, and the *dashed lines* represent direct measurements of velocities. *Black lines* represent how Line W is extended in the model to obtain a closed observing system. *Red lines* indicate additional moorings needed to capture the standing eddy. **b** Time series of the AMOC (*red*), its reconstruction (*blue*) based on Line W mimicking the array in the Atlantic (without red moorings of **a**) and its reconstruction (*gray*) based on eastward extended Line W (with red moorings of **a**) at 1,000 m. **c** Vertical time mean profile of the AMOC (*red*) and its reconstructions (*blue*, *gray*). **d** Hovmoeller diagram of the AMOC minus its reconstruction (as in *blue line* in **b** and **c**) showing the absolute error

Line W, we simulate the use of the RAPID array east of the westernmost MAR mooring (26°N_{East}) and the existing observations at Bermuda (Line W-B-RAPID, Fig. 10a). From a density profile at every grid cell, the reconstructed AMOC shows a RMSE of 2.2 Sv against the modeled AMOC (Fig. 10b–d). The AMOC has a time mean value of 12.5 Sv with a STD of 6 Sv, and the reconstruction has a time mean value of 11.1 Sv with a STD of 5.6 Sv. Though the RMSE is slightly larger than for the Line W-32°N reconstructions, we proceed to deploy a setup for a Line W and RAPID based observing system which is practicable in reality since the visual impression supported by the correlation coefficient of 0.96 still suggests that the variability is largely captured.

Similar to 26°N and Line W-32°N, we reduce the number of profiles to a feasible amount. At 26°N_{East}, we use the same profiles as for the simulation of RAPID/MOCHA. For the remaining gap between Bermuda and the RAPID MAR mooring, we assume that a station as Hydrostation 'S' (e.g., Phillips and Joyce, 2007) can be used, where measurements of temperature and salinity are taken biweekly to about 3,300 m deep. Using profiles along the line, the mid-ocean component is obtained from thermal wind balance. Six profiles are used for the observing system based on Line W, B-MAR, and 26°N_{East} (Fig. 10a). The reconstruction of the AMOC has a time mean value of 11.2 Sv with a STD of 5.7 Sv, leaving a bias of 1.3 Sv, and a RMSE of 2.3 Sv. In the vertical, the AMOC is nearly completely reconstructed (Fig. 10e–g), though this is likely due to a cancelation of errors, as the vertical profile for the maximum number of density profiles shows a bias at depth (Fig. 10c, d).

(7) *LineW-B-RAPID based on a realistic Line W western boundary array* As for Line W-32°N, an observing system with a realistic setup of Line W comprising the extended Line W array (Section 3.2(4)), measurements at Bermuda and from the 26°N RAPID array is now tested. This setup relies on a number of moorings which exist in real world at Line W and RAPID/MOCHA, and uses only a few additional, supplementary profiles (Fig. 11a). The resulting reconstructed AMOC ($\psi_{rec}^{w/26} = 16.0 \pm 4.8$ Sv) overestimates the AMOC by about 3.5 Sv (Fig. 11b); likewise, the RMSE is 5.1 Sv. Similarly, the AMOC is overestimated in all depth layers (Fig. 11c, d). The correlation coefficient of 0.79 still suggests a reasonable estimate of the AMOC based on direct measurements of velocity and the thermal wind for the western boundary transport at Line W. Using further direct velocity observations of the standing eddy, the reconstruction is improved, although the overestimation of the WBC is obvious in the overestimated AMOC

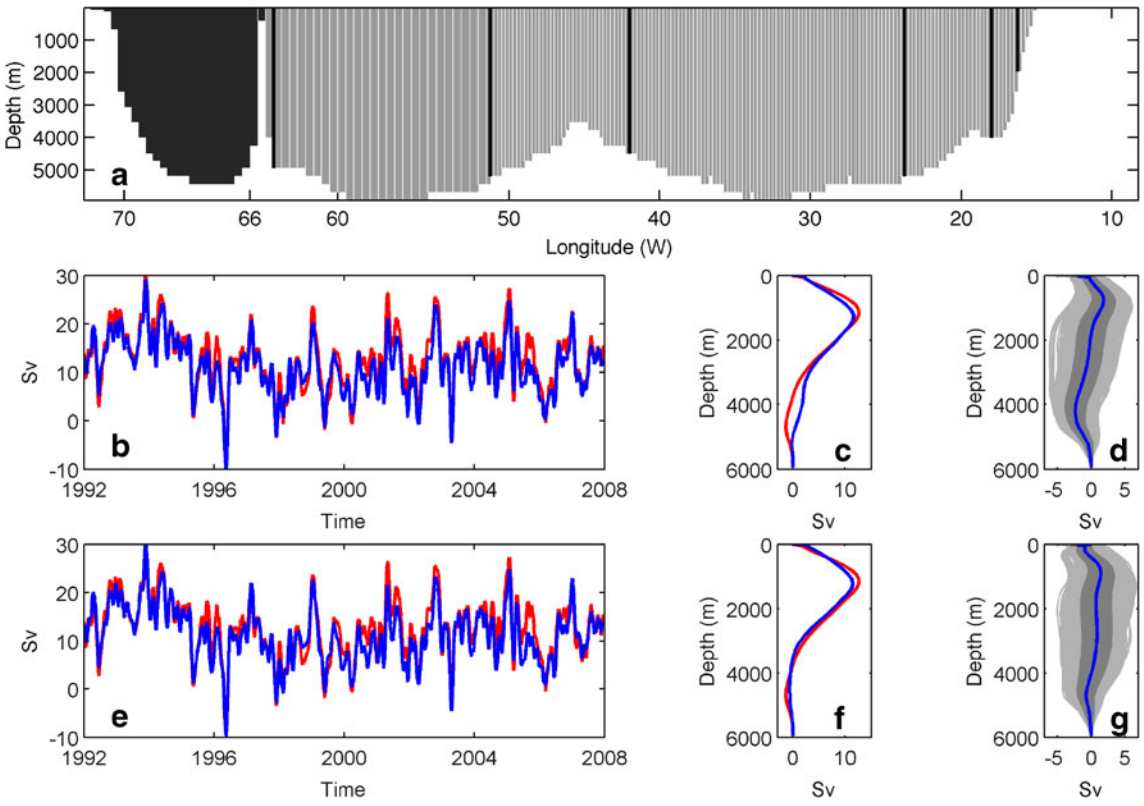

Fig. 10 AMOC at LineW-B-RAPID and its reconstruction: **a** Topography with six placed density profiles (*black*). *Dark gray area* shows the transect of Line W where the velocity field is assumed to be completely known. **b** Time series of the AMOC (*red*) and its reconstruction based on 173 profiles at every grid cell (*blue*). **c** Vertical time mean profile of the AMOC (*red*) and its reconstruction (*blue*). **(d)** Vertical profile of the AMOC minus its reconstruction showing the absolute error. STD in *dark gray*. **e** Time series of the AMOC (*red*) and its reconstruction based on the six profiles (*blue*). **f** Vertical time mean profile of the AMOC (*red*) and its reconstruction (*blue*). **g** Vertical profile of the AMOC minus its reconstruction showing the absolute error. STD in *dark gray*

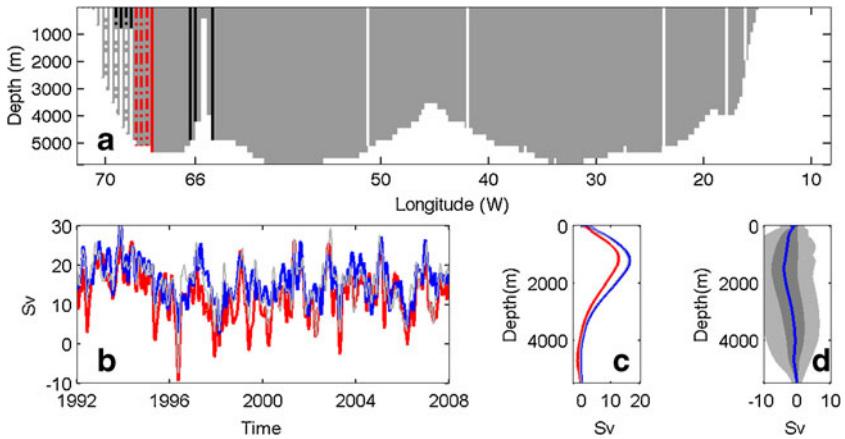

Fig. 11 AMOC at Line W-B-RAPID and its estimate based on measurements at Line W and in the mid-ocean: **a** Topography with placed density profiles. *White lines* represent existing observations at Line W and RAPID/MOCHA, where the *solid lines* are used to measure T and S, and the *dashed lines* represent direct measurements of velocities. *Black lines* represent, how Line W is extended in the model to obtain a closed observing system. *Red lines* indicate additional moorings needed to capture the standing eddy. **b** Time series of the AMOC (*red*), its reconstruction (*blue*) based on Line W as presently deployed in the Atlantic (without red moorings of **a**) and its reconstruction (*gray*) based on eastward extended Line W (with red moorings of **a**) at 1,000 m. **c** Vertical time mean profile of the AMOC (*red*) and its reconstructions (*blue*,*gray*). **d** Vertical profile of the AMOC minus its reconstruction showing the absolute error

(RMSE of 4.1 Sv, correlation of 0.86, Fig. 11b). While these tests indicate that closing Line W with an observing system mostly based on existing observations (i.e., RAPID) leads to a reasonable reconstruction of the AMOC in the model, the question remains to what extent this would be an AMOC reconstruction independent of the 26°N AMOC reconstruction.

(8) *LineW-B-RAPID against 26°N with a time-mean WBC* The WBC has a strong influence on the AMOC variability at both sections Line W-B-RAPID and 26°N. To asses how independent 26°N is from Line W-B-RAPID and to evaluate the relation between the reconstructed mid-ocean component of the two transects, we subtract the Ekman component from the total AMOC and hold the WBC temporally constant, so that the resulting transport variability is basically given by $\psi^{w/26} - \psi_{ek}^{w/26} - \psi_{\mathrm{wbc}}^{w/26}$. Analogously to the previous analysis of Line W-32°N, the WBC component at Line W is set to its time mean value of 31 Sv. Similarly, the WBC component at 26°N is set to its mean value of about 31 Sv. The resulting AMOC at 26°N and Line W-B-RAPID, containing only the variability of the mid-ocean transport based on the thermal wind balance, shows no significant relation between both sections (correlation coefficient of 0.47, Fig. 12a). The AMOC at 26°N exceeds the Line W-B-RAPID AMOC by about 4 Sv. From the reconstruction of the mid-ocean component, we obtain no significant relation between both sections (correlation coefficient of 0.41, blue and orange lines in Fig. 12b, c).

Aiming to separate the influence of the eastern boundary, which is commonly used in both the 26°N and the Line W-B-RAPID AMOC estimate, we analyze the variability at $26°\mathrm{N}_{East}$ in relation to the western boundary variability and the total mid-ocean variability of the sections 26°N and Line W-B-RAPID. In addition to the above redefinition of the AMOC, the $26°\mathrm{N}_{West}$ and B-MAR section are now set to their time-mean value for this analysis to obtain the variability of the eastern boundary array at 26°N. At $26°\mathrm{N}_{East}$, the eastern boundary transport based on the model velocity field shows clear interannual variability at both sections Line W-B-RAPID and 26°N. In the reconstructed AMOC, mostly the seasonal cycle emerges, while the interannual variability cannot be obtained from the density field (Fig. 13a, b). This confirms the result of Bingham and Hughes (2008), who have shown that on timescales longer than 1 year, the eastern boundary can be neglected and variations of the AMOC can be obtained from bottom pressure variations at the western boundary at 42°N.

At 26°N, analyzing the contribution of the eastern and western boundary transport fluctuations based on density field reveals that eastern and western boundary contribute both significantly to the variability of the mid-ocean transport in terms of standard deviation, although the western boundary transport has a slightly higher STD than the eastern boundary (1.7–1.2 Sv). Similar findings have been attained from RAPID/MOCHA observations by (Chidichimo et al. 2010) from analysis of the eastern and western boundary density and transport fluctuations,

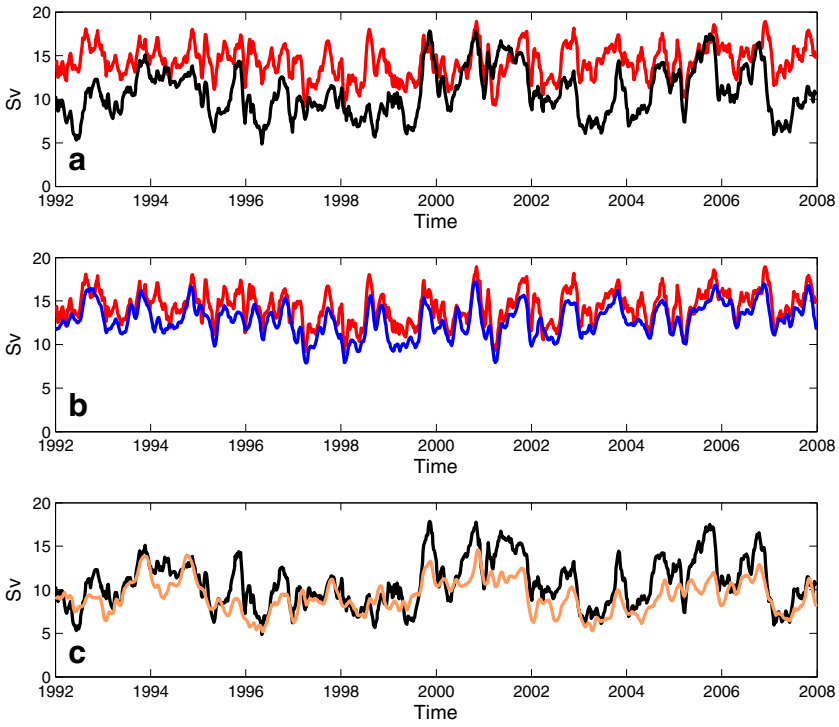

Fig. 12 AMOC at Line W-B-RAPID: **a** Time series of the AMOC at Line W-B-RAPID (*black*) and 26°N (*red*) with a time-mean WBC component. **b** 26°N: AMOC (*red*) and its reconstruction (*blue*) with a time-mean WBC component. **c** Line W-B-RAPID: AMOC (*black*) and its reconstruction (*orange*) with a time-mean WBC component

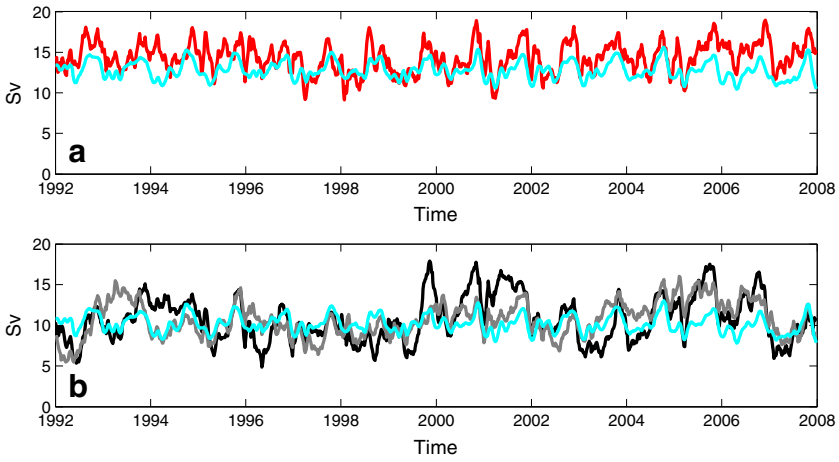

Fig. 13 AMOC at 26°N and Line W-B-RAPID: **a** 26°N: AMOC (*red*) and its reconstruction (*cyan*) at 26°N with a time-mean WBC component and a time-mean $26°N_{West}$ component. **b** Line W-B-RAPID: AMOC with a time-mean WBC component (*black*), AMOC (*gray*), and its reconstruction (*cyan*) with a time-mean WBC component and a time-mean B-MAR component between Bermuda and RAPID.

but in the observations, the eastern and western boundary contribute almost equally to the variability in terms of the standard deviation. At Line W-B-RAPID, the western boundary (section B-MAR) clearly shows a higher variability than the eastern boundary $26°N_{East}$ (STD of 2.3–1.2 Sv) introducing interannual variability into the total mid-ocean transport. Due to the high influence of the western boundary variability on the full mid-ocean transport resulting from the density field at the section Line W-B-RAPID, the relation to the mid-ocean variability at 26°N is low (correlation coefficient of 0.41).

Although both, the 26°N and the Line W-B-RAPID section, use the eastern boundary moorings of RAPID ($26°N_{East}$), which induces mostly the seasonal cycle into the reconstructed AMOC, the relation between the 26°N and the Line W-B-RAPID section is low. The major influence on the interannual variability of the interior transport at Line W-B-RAPID comes from the reconstructed western mid-ocean transport near Bermuda, leading to an evident relation to the Line W-32°N section (not shown, correlation coefficient 0.91).

4 Discussion

Both simulated observing systems at Line W-32°N, as well as at Line W-B-RAPID capture the main characteristics of the AMOC in the model. Hence, the exact setup of a Line W-based observing system is—at least in the model—not critical. However, a few limitations arise due to the restriction of the model to represent the real—or rather observed—AMOC variability.

Analyzing the two Line W-based sections, we find a high influence of the WBC on the AMOC variability. In the model, we cannot find any significant relation between the variability at 26°N and the two Line W-based sections based on transport comparisons partitioned by depth. We further find that the variability is also increased in the latitudes of Line W for zonal sections, although the variability of the transport across Line W exceeds that of the zonal sections due to a higher influence of the zonal flow and the change of pressure gradients by passing transient eddies. Further, the unrealistic Hatteras eddy in ORCA025 increases the variability and induces an ageostrophic contribution into the velocity field at Line W which has to be taken into account for our simulations. For other angled sections, the variability of the AMOC is in the order of pure zonal sections. Whether the observed transports are related is—at this point—unclear. As proposed by (Toole et al. 2011), a comparison of Line W and RAPID/MOCHA at 26°N based on density classes would be a physically more meaningful approach, since stratification varies much between 26°N and 40°N at the northern edge of Line W. Besides, the effect of the eddy field on the variability of the AMOC raises again the question how eddies influence the variability we see in actual measurements and how we can tackle the impact of the eddy field in observations. But this issue goes beyond the scope of this study and is left for future work.

The tested observing systems for reconstructing the AMOC are based on Line W observations measuring the WBC component, which cover the continental slope south of New England with a moored array. However, the Line W measurement program is designed to quantify the DWBC. The total meridional transport including the northward directed Gulf Stream is only sampled during occasional cruises (Toole et al. 2011), so that an almost perfect observation of the WBC, as cable measurements provide in the Florida Straits at 26°N, is not given at Line W. Thus, our first assumption of a known WBC transport at Line W in the model is too optimistic. But the implementation of a realistic Line W array, providing temperature and salinity measurements, as well as direct current meter observations at the continental slope south of New England, leads, together with extending Line W to the surface and deploying to

additional moorings at the Bermuda Rise, to a sensible estimate of the WBC between New England and Bermuda, with the restriction that we have to assume a known velocity field in the area of the standing eddy in the model.

For an observing system based on Line W, RAPID/MOCHA, and observations at Bermuda, it is debatable whether the temporal resolution of the measurements at Hydrostation 'S' (taken biweekly, c.f. Phillips and Joyce, 2007) is sufficient for a continuous AMOC monitoring strategy in reality.

For both Line W-based observing systems, we find a reasonable reconstruction of the AMOC. Reducing the number of profiles to a thinned array using only few profiles at the boundaries, we find a good reconstruction of the AMOC. As a lot of density information is lost by thinning out the profiles of the setup, an improved reconstruction is a result of a cancelation of errors. In particular, the AMOC reconstruction based on the full density field reveals that bottom velocities are mostly underestimated by the method. Thus, a better representation of bottom velocities and the deep return flow by using fewer density profiles is unlikely. However, even with several adaptations that would have to be made at Line W for a real observing system, the present simulations are a reference point for a Line W-based AMOC observing system.

5 Conclusions

Based on our observing system simulations for the AMOC in ORCA025, we conclude:

- The existing Line W western boundary array allows with its extension to the surface and to the east and additional moored observations at Bermuda a reasonable measurement of the transport at the western boundary between New England and Bermuda.
- Supplementing Line W with observations across 32°N and with RAPID/MOCHA observations at 26°N yield independent estimates of the AMOC variability at interannual timescales.
- An observing system based on Line W and 32°N (Line W-32°N) provides reasonable results in the model, although poorly captured bottom velocities yield an underestimated AMOC in deep layers.
- An observing system combining existing measurements of Line W and RAPID/MOCHA provides a reliable AMOC reconstruction, having the advantage that existing instruments could be used with relatively small effort.
- An observing array based on Line W and RAPID/MOCHA as before could potentially provide an AMOC estimate largely independent of the 26°N AMOC variability: the AMOC variability is dominated by the western boundary variability at interannual timescales, while the eastern mid-ocean contribution mostly introduces the seasonal cycle in the reconstructed AMOC.

Acknowledgments We thank John Toole for providing information about Line W and valuable scientific discussions. We thank both reviewers for their constructive and valuable comments which helped to significantly improve the manuscript. This work was supported by the Cooperative Project "RACE - Regional Atlantic Circulation and Global Change" funded by the German Federal Ministry for Education and Research (BMBF), 03F0651A, and by the CliSAP Cluster of Excellence at the University of Hamburg funded through the Deutsche Forschungsgemeinschaft (M.F. and J.B.). The research leading to the presented results has received funding from the European Union's Seventh Framework Programme (FP7/2007-2013) under grant agreement no 212643 (EU-THOR) (A.B., E.B). The model integration was performed at the North-German Supercomputing Alliance (HLRN). Data from the RAPID-WATCH MOC monitoring project are funded by the Natural Environment Research Council and are freely available from http://www.noc.soton.ac.uk/rapidmoc.

References

Baehr J, Hirschi J, Beismann J, Marotzke J (2004) Monitoring the meridional overturning circulation in the North Atlantic: a model-based array design study. J Mar Res 62(3):283–312

Barnier B, Madec G, Penduff T, Molines JM, Treguier AM, Beckmann A, Biastoch A, Böning C, Dengg J, Derval C, Durand E, Gulev S, Le Sommer J, Remy E, Talandier C, Theetten S, Maltrud M (2006) Impact of partial steps and momentum advection schemes in a global ocean circulation model at eddy permitting resolution. Ocean Dyn 56:543–567. doi:10.1007/s10236-006-0082-1

Biastoch A, Böning CW, Getzlaff J, Molines JM, Madec G (2008) Causes of inter-annual-decadal variability in the meridional overturning circulation of the midlatitude North Atlantic Ocean. J Clim 21:6599–6615. doi:10.1175/2008JCLI2404.1

Bingham RJ, Hughes CW (2008) Determining North Atlantic meridional transport variability from pressure on the western boundary: a model investigation. J Geophys Res 113:C09008. doi:10.1029/2007JC004679

Bingham RJ, Hughes CW, Roussenov V, Williams RG (2008) Meridional coherence of the North Atlantic meridional overturning circulation. Geophys Res Lett 34:L23606. doi:10.1029/2007GL031731

Chidichimo M, Kanzow T, Cunningham S, Johns W, Marotzke J (2010) The contribution of eastern-boundary density variations to the Atlantic meridional overturning circulation at 26.5°N. Ocean Sci 6:475–490

Cunningham S, Kanzow T, Rayner D, Baringer M, Johns W, Marotzke J, Longworth H, Grant E, Hirschi J, Beal L et al. (2007) Temporal variability of the Atlantic meridional overturning circulation at 26.5°N. Science 317:935–938

Cunningham S et al. (2010) The present and future system for measuring the Atlantic meridional overturning circulation and heat transport. In: Hall J, Harrison D E, Stammer D (eds) Proceedings of OceanObs'09: sustained ocean observations and information for society, September 2009, vol 2. ESA Publication WPP-306, Venice, pp. 21-25. doi:10.5270/OceanObs09.cwp.21

The DRAKKAR Group, Barnier B, Brodeau L, Le Sommer J, Molines JM, Penduff T, Theetten S, Treguier AM, Madec G, Biastoch A,

Böning C, Dengg J, Gulev S, Bourdallé Badie R, Chanut J, Garric G, Alderson S, Coward A, de Cuevas B, New A, Haines K, Smith G, Drijfhout S, Hazeleger W, Severijns C, Myers P (2006) Impact of partial steps and momentum advection schemes in a global ocean circulation model at eddy permitting resolution. Ocean Dyn 56:543–567. doi:10.1007/s10236-006-0082-1

Goosse H, Fichefet T (1999) Importance of ice-ocean interactions for the global ocean circulation: a model study. J Phys Oceanogr 104(C10):23,337–23,355. doi:10.1029/1999JC900215

Hirschi J, Baehr J, Marotzke J, Stark J, Cunningham S, Beismann J (2003) A monitoring design for the Atlantic meridional overturning circulation. Geophys Res Lett 30(7):1413. doi:10.1029/2002GL016776

Jackett DR, McDougall TJ (1995) Minimal adjustment of hydrographic data to achieve static stability. J Atmos Ocean Technol 12:381-389

Kanzow T, Cunningham S, Rayner D, Hirschi J, Johns W, Baringer M, Bryden H, Beal L, Meinen C, Marotzke J (2007) Observed flow compensation associated with the MOC at 26.5°N in the Atlantic. Science 317(5840):938-941. doi:10.1126/science.1141293

Kanzow T, Johnson HL, Marshall DP, Cunningham S, Hirschi J, Mujahid A, Bryden H, Johns W (2009) Basinwide integrated volume transports in an eddy-filled ocean. J Phys Oceanogr 39:3091–3110. doi:10.1175/2009JPO4185.1

Kanzow T, Cunningham S, Johns W, Hirschi J, Marotzke J, Baringer M, Meinen C, Chidichimo M, Atkinson C, Beal L, Bryden H, Collins J (2010) Seasonal variability of the Atlantic meridional overturning circulation at 26.5°N. J Clim 23(21):5698–5678. doi:10.1175/2010JCLI3389.1

Large WG, Yeager S (2009) The global climatology of an interannually varying air-sea flux data set. Clim Dyn 33:342–364

Lee T, Marotzke J (1998) Seasonal cycles of meridional overturning and heat transport of the Indian Ocean. J Phys Oceanogr 28:923–943. doi:10.1175/1520-0485(1998)0280<923:SCOMOA>2.0.CO;2

Madec G (2008) NEMO reference manual, ocean dynamics component : NEMO-OPA. Preliminary Version, Tech. Rep. 27, Note du Pôle de modélisation, Institut Pierre-Simon Laplace (IPSL). France, ISSN No 1288–1619, 2008

Marotzke J, Giering R, Zhang K, Stammer D, Hill C, Lee T (1999) Construction of the adjoint MIT ocean general circulation model and application to Atlantic heat transport sensitivity. J Geophys Res 104:29,529–29,547. doi:10.1029/1999JC900236

Phillips H, Joyce T (2007) Bermuda's tale of two time series: Hydrostation S and BATS. J Phys Oceanogr 37:554–571. doi:10.1175/JPO2997.1

Toole JM, Curry R, Joyce T, McCartney M, Peña-Molino BP (2011) Transport of the North Atlantic Deep Western Boundary Current about 39°N, 70°W: 2004-2008. Deep-Sea Res II 58(2011):1768–1780. doi:10.1016/j.dsr2.2010.10.058

Willis J (2010) Can in situ floats and satellite altimeters detect long-term changes in Atlantic Ocean overturning. Geophys Res Lett 37:L06602. doi:10.1029/2010GL042372